Diffusion and Perfusion Magnetic Resonance Imaging, edited by D. Le Bihan.
Raven Press, Ltd., New York 1995.

CHAPTER 1

Molecular Diffusion and Nuclear Magnetic Resonance

Denis Le Bihan and Peter J. Basser

The purpose of this chapter is to review how molecular diffusion can be measured using nuclear magnetic resonance (NMR). The concept of molecular diffusion is introduced, and various methods to measure it are motivated from the basic equations governing diffusive transport. The measurement of molecular diffusion using NMR is presented. The effect of molecular diffusion on the NMR signal is described, and each paradigmatic pulse sequence used to measure diffusion with NMR is introduced. In the following chapters, these pulse sequences will be described in more detail, especially in the context of NMR imaging (see Chapter 2). Finally, we discuss specific problems encountered when studying diffusion in biological tissues. These problems will be analyzed more thoroughly in Chapters 7 and 8.

THE MOLECULAR DIFFUSION PROCESS

Diffusive transport is readily observed in steady-state, non-equilibrium systems, such as in cells. Here, a concentration difference is established between two compartments, and a macroscopic diffusive flux can be observed between them. Fick's law describes how the molecular flux density $\mathbf{J}$, depends on the molecular concentration gradient, ∇C (1):

$$\mathbf{J} = -D\nabla C \qquad [1]$$

The diffusion coefficient, D, is a proportionality constant that can be determined experimentally from the ratio of the flux and the concentration gradient, measured using either physical or chemical methods (2). By combining the equation of conservation of mass,

$$\frac{\partial C}{\partial t} = -\nabla \cdot J \qquad [2]$$

with Fick's law, one obtains the diffusion equation:

$$\frac{\partial C}{\partial t} = -\nabla \cdot J = \nabla \cdot (D\nabla C). \qquad [3]$$

For a constant (spatially uniform) diffusivity, solutions are readily obtained for various paradigmatic initial concentration profiles and boundary conditions. For example, the solution of the diffusion equation in an unbounded medium for particles satisfying the initial condition $C(\mathbf{r}, 0) = \delta(\mathbf{r} - \mathbf{r}_0)$ is (2):

$$C(\mathbf{r}, t) = \left(\frac{1}{\sqrt{4\pi Dt}}\right)^3 \exp\left(\frac{-(\mathbf{r} - \mathbf{r}_0)\cdot(\mathbf{r} - \mathbf{r}_0)}{4Dt}\right) \qquad [4]$$

The diffusion equation suggests other well-known methods to determine D employing radioactive or fluorescent tracers. Here, the concentration profiles of the tracer are monitored over time, and its diffusivity is inferred from them (1). Microscopic displacements can be seen with tracers on the scale of millimeters. Spatially resolved methods can also be used, such as infrared spectroscopy or Rayleigh scattering (3), allowing resolution in the micrometer range. Such tracer techniques have been successfully applied in biological systems, such as the brain (4,5). However, because of the inherent invasiveness of using exogenous tracers, such techniques cannot be used *in vivo* with humans.

An alternative approach to measuring diffusivity is to monitor the diffusion process itself, i.e., the random

D. Le Bihan: Department of Diagnostic Radiology, Warren G. Magnuson Clinical Center, National Institutes of Health, Bethesda, Maryland 20892.

P. J. Basser: Bioengineering and Instrumentation Program, National Center for Research Resources, National Institutes of Health, Bethesda, Maryland 20892.

motions of an ensemble of particles. Einstein (6) showed that the diffusion coefficient measured in the nonequilibrium concentration cell experiments described above is the same quantity that appears in the variance of the conditional probability distribution, $P(\mathbf{r} \mid \mathbf{r}_0, t)$, the probability of finding a molecule at a position $\mathbf{r}$ at a time t, which was initially at a position $\mathbf{r}_0$. For free diffusion, this conditional probability distribution obeys the same diffusion equation as the particle concentration given. It follows that

$$\langle (\mathbf{r} - \mathbf{r}_0) \cdot (\mathbf{r} - \mathbf{r}_0) \rangle = 6\,Dt \qquad [5]$$

The Einstein equation, which relates D to the root mean square of the diffusion distance (Fig. 1), suggests that by measuring the second moment of the conditional probability distribution of the diffusing species, one could infer the diffusivity directly. This approach is amenable to measurements using NMR methods.[1] In fact, NMR provides the only existing method with which to characterize molecular displacements over distances larger than the mean free path. This justifies the considerable success of diffusion NMR in physics and chemistry. In some cases, when it is desirable to monitor individual molecular pathways (for instance in terms of mean elementary diffusion steps) NMR must be replaced by other techniques, although some information can be derived from relaxation NMR studies. The relaxation times T_1 and T_2 depend to some extent on diffusion-driven molecular mobility, as can be seen in the Bloom-Purcell-Bloembergen equations (7,8). However, T_1 and T_2 are influenced by many other processes besides diffusion, so that this approach is extremely indirect. It may be inferred that T_1 or T_2 are generally not suitable for estimating diffusivity. In biological tissues, the diffusion mechanism that predominates for relaxation is rotational, not translational diffusion. One may thus expect to see that T_1 or T_2, and diffusive relaxation are different in tissues.

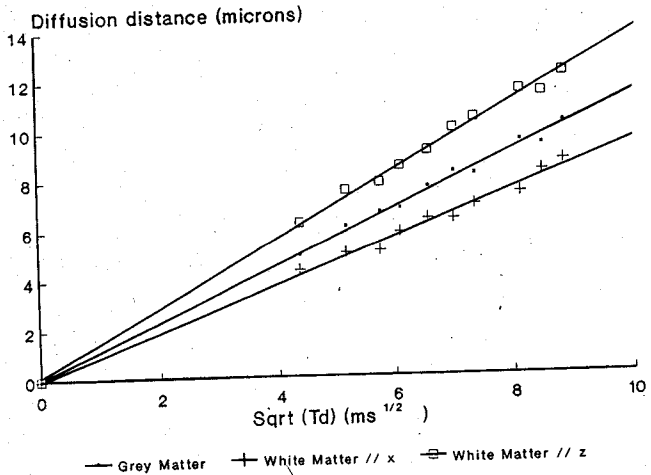

FIG. 1. Diffusion distance versus diffusion time in human brain. The diffusion distance (root mean square displacement) of diffusing water molecules is plotted against the square root of the diffusion time, T_d. This diffusion distance was calculated according to Einstein's relation (Eq. [5]) from diffusion coefficients measured at 1.5T for different diffusion times in human brain *in vivo*. The plot is linear, as is expected for free diffusion. The slope gives the diffusion coefficient. In white matter, molecular displacements and diffusion were evaluated both parallel to (z) and perpendicular to (x) the myelin fiber direction to take into account diffusion anisotropy.

[1] N.B. One must replace the diffusion constant by a diffusion tensor in Eq. [5] when inferring molecular displacements in tissues in which diffusion exhibiting anisotropic diffusion, i.e., the molecular mobility appears to be different in the x, y, or z directions (1).

The methods to measure diffusion at microscopic length scales are limited. Laser and neutron scattering techniques are both unsuitable for *in vivo* human studies. Owing to the high degree of photon scattering in turbid tissues, light scattering is not an efficient means to probe diffusivity *in vivo*, except, perhaps, superficially (9). Moreover, it is limited in spatial resolution to a few microns by the wavelength of the laser beam used. Neutron scattering allows a spatial resolution in the nanometer range, which is highly desirable for probing biological tissues at the molecular scale; but its obvious main limitation, for any *in vivo* application is that it requires neutron beams. To conclude this section, we are fortunate that NMR is available as a tool for the completely noninvasive investigation of molecular displacements in the micron range (and possibly the sub-micron range) encompassing the size of most biological tissue structures.

DIFFUSION AND NMR

The Basic Principles

The effect of diffusion on the NMR signal can be understood from a simple bipolar pulsed gradient experiment (Fig. 2). The purpose of these gradient pulses is to magnetically label spins carried by molecules. Let us denote G as the gradient strength, δ as the gradient duration, and Δ as the time interval between the pulse onsets (following Stejskal and Tanner's terminology) (10). The first gradient pulse induces a phase shift ϕ_1 of the spin transverse magnetization, which depends on the spin position (spin labeling). If the gradient is along z:

$$\phi_1 = \gamma \int_0^{\delta} G z_1 dt = \gamma G \delta z_1 \qquad [6]$$

where z_1 is the spin position supposed to be constant during the short duration δ of the gradient pulse γ is the gyromagnetic ratio. After the 180° rf pulse, ϕ_1 is transformed into $-\phi_1$. Similarly, the second pulse will produce a phase shift ϕ_2 (spin unlabeling):

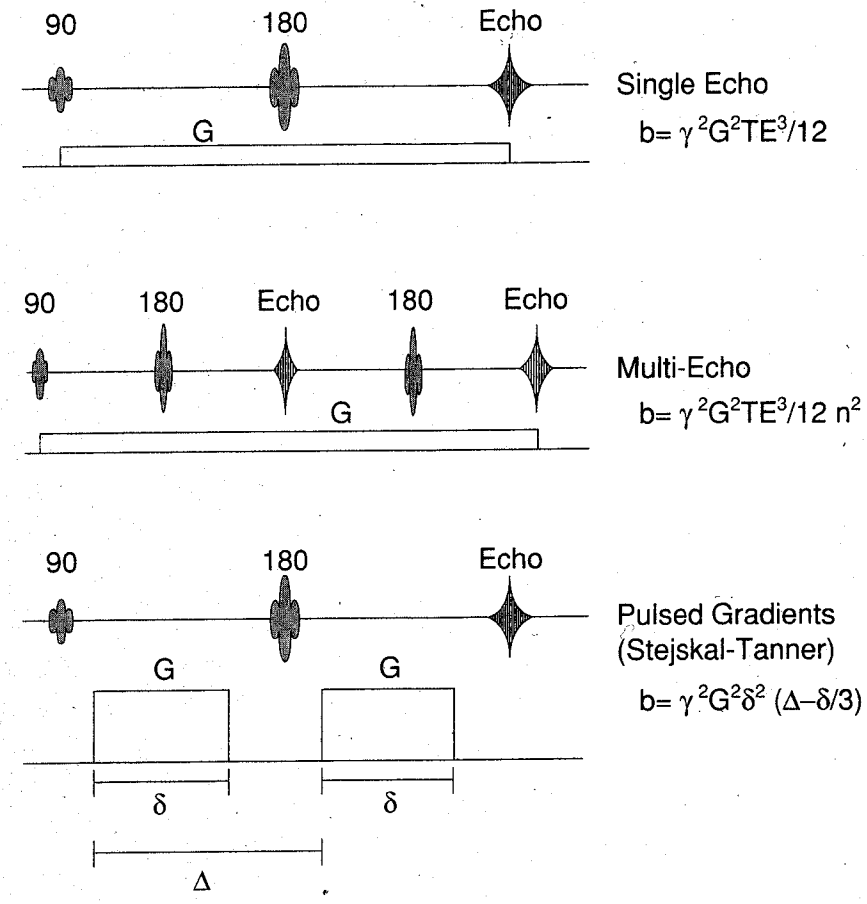

FIG. 2. Effect of diffusion for different gradient pulse schemes. The spin-echo signal attenuation due to diffusion depends largely on the gradient pulse scheme used. The gradient contribution is characterized by a gradient factor b, such that the signal attenuation is $\exp(-bD)$, where D is the diffusion coefficient. The largest effect is produced by a constant gradient pulse, G, in a single echo sequence. However, the Stejskal-Tanner scheme, i.e., gradient pulses of short duration δ, separated by a time interval D, is better suited for imaging and has a better defined diffusion time.

$$\phi_2 = \gamma \int_{\Delta}^{\Delta+\delta} G z_2 dt = \gamma G \delta z_2 \qquad [7]$$

where z_2 is the spin position during the second pulse. The net dephasing, $\delta(\phi)$, is therefore:

$$\delta(\phi) = \phi_2 - \phi_1 = \gamma G \delta (z_1 - z_2). \qquad [8]$$

One immediately sees that for "static" spins $z_1 = z_2$, so that the bipolar gradient pair produces no net dephasing. For "moving" spins, however, there is a net dephasing that will depend on the spin history during the time interval Δ between the pulses, and which will affect the transverse magnetization. We also see that the position of the two gradient pulses in each half of the spin-echo sequence does not matter, it is the time elapsed between them that affects the net phase. We measure the total magnetization—the vector sum of the magnetic moments of the individual nuclei, which may have different motion histories:

$$\frac{M}{M_0} = \sum_{j=1}^{N} \exp\,(i\delta(\phi_j)). \qquad [9]$$

This sum can be evaluated once the net phase distribution is known. Assuming free diffusion in a homogenous domain, the probability of finding a spin at position z_1 is a constant. If $P(z_2\, z_1, \Delta)dz_2$ is the conditional probability of finding a spin initially at z_1 between positions z_2 and $z_2 + dz_2$ after a time interval Δ, the amplitude attenuation is:

$$\frac{M}{M_0} = \int_{-\infty}^{\infty}\int_{-\infty}^{\infty} \exp(i\gamma G\delta(z_1 - z_2)) \times P(z_2 \mid z_1, \Delta)\, dz_1 dz_2 \qquad [10]$$

For free diffusion in one dimension, the conditional probability is given by:

$$P(z_2 \mid z_1, \Delta) = \frac{1}{\sqrt{4\pi D\Delta}} \exp\left(\frac{-(z_1 - z_2)^2}{4D\Delta}\right) \qquad [11]$$

where D is the diffusion coefficient. Combining Eqs. [10] and [11], we obtain:

$$\frac{M}{M_0} = \exp(-(\gamma G\delta)^2\, D\Delta) \qquad [12]$$

Either Eq. [12] or its logarithm,

$$\ln\left(\frac{M}{M_0}\right) = -(\gamma G\delta)^2\, \Delta D \qquad [13]$$

relates the measured signal attenuation to the diffusivity, and is the basis for diffusion measurement using NMR.

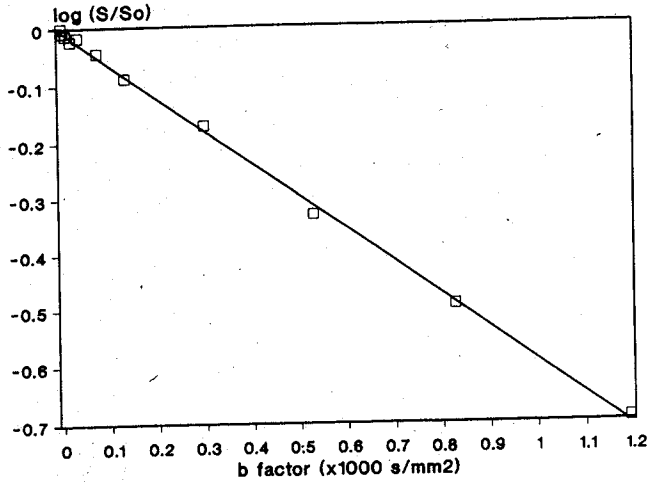

FIG. 3. Effect of diffusion on spin-echo signal amplitude. The logarithm of the signal intensity obtained in white matter was plotted against the gradient factor b, according to Eq. [15]. The plot is linear, and the slope is equal to the diffusion coefficient ($D = 0.60 \pm 0.01 \times 10^{-3}$mm^2/s). (Data obtained at 4.7T in the *In Vivo* NMR Center, NIH, in collaboration with C. T. W. Moonen and P. C. M. van Zijl.)

According to Eq. [13], we may estimate the diffusion coefficient (or diffusion distances) by varying G or δ and measuring the slope of the logarithm of the signal intensity versus $(G\delta)^2$ (Fig. 3). Two problems still remain with this simplified approach. First, δ may not be negligible as compared to Δ, so that diffusion occurring during the application of the gradient pulses can no longer be ignored. This is the case for commercial MRI units in which the maximum available gradient strength is generally limited, so that long gradient durations are required to produce observable diffusion effects. Second, there may be additional gradient pulses, including imaging pulses and background residual gradients that also affect the measured magnetization. To address these problems, we must solve the Bloch-Torrey equation (11), for a general pulse sequence.

Equations Governing the Diffusive Transport of Magnetization

The Bloch equations (12) with diffusion (11) relate the applied magnetic field vector, $\mathbf{B} = (B_x, B_y, B_z)$ to the net (nuclear) magnetization vector, $\mathbf{M} = (M_x, M_y, M_z)$ in the laboratory frame of reference:

$$\frac{\partial \mathbf{M}}{\partial t} = \gamma \mathbf{M} \times \mathbf{B} - \begin{pmatrix} \frac{1}{T_2} & 0 & 0 \\ 0 & \frac{1}{T_2} & 0 \\ 0 & 0 & \frac{1}{T_1} \end{pmatrix} \mathbf{M} + \mathbf{M}_0 \begin{pmatrix} 0 \\ 0 \\ 1/T_1 \end{pmatrix} + \nabla\cdot(\underline{D}\nabla\mathbf{M}). \quad [14]$$

Above, γ is the gyromagnetic ratio, T_1 and T_2 are the longitudinal and transverse relaxation times, and $\mathbf{M}_0$ is the equilibrium magnetization in the direction of the static applied magnetic field, $\mathbf{B}_0$.

For a 90°–180° spin-echo sequence, the spins are subjected to an impressed static magnetic field superposed with a linear gradient in the z direction (7):

$$\mathbf{B}(\mathbf{r}, t) = (0, 0, \mathbf{r}\cdot\mathbf{G}(t) + B_0)^T \quad [15]$$

where $\mathbf{r}$ is the displacement vector, and

$$\mathbf{G}(t) = (G_x(t), G_y(t), G_z(t))^T. \quad [16]$$

Then, the Bloch equations (12) for the complex-valued transverse magnetization, m:

$$m(\mathbf{r}, t) = M_x(\mathbf{r}, t) + i\, M_y(\mathbf{r}, t) \quad [17]$$

can be recast as a transport equation for m (11):

$$\frac{\partial m}{\partial t} = -i\omega_0 m - \frac{m}{T_2} - i\gamma\mathbf{r}\cdot\mathbf{G}(t)m + \nabla\cdot(\underline{D}\nabla m) \quad [18]$$

where the Larmor relation, $\gamma B_0 = \omega_0$, was used.

To eliminate the attenuation due to transverse relaxation and signal modulation by Larmor precession, the following substitution is used:

$$m(\mathbf{r}, t) = \psi(\mathbf{r}, t) \exp\left(-\left(i\omega_0 + \frac{1}{T_2}\right) t\right) \quad [19]$$

so that

$$\frac{\partial \psi}{\partial t} = -i\gamma\mathbf{r}\cdot\mathbf{G}(t)\psi + \nabla\cdot(\underline{D}\nabla\psi) \quad [20]$$

For a spin-echo sequence, one can further simplify the transport equation by separating $\psi(\mathbf{r}, t)$ into an imaginary part, which represents the solution to Eq. [20] without diffusion, and a real, time-dependent part that represents the attenuation due to diffusion:

$$\psi(\mathbf{r}, t) = M(t) \exp(-i\mathbf{r}\cdot\mathbf{k}(t)) \quad [21]$$

where

$$\mathbf{k}(t) = \gamma \int_0^t \mathbf{G}(t')\, dt'. \quad [22]$$

The resulting equation for $M(t)$ is:

$$\frac{dM}{dt} = M(t)\nabla\cdot(\underline{D}\nabla \exp(-i\mathbf{r}\cdot\mathbf{k}(t))) \quad [23]$$

$$= -M(t)\, \mathbf{k}(t)^T\, \underline{D}\mathbf{k}(t)$$

which has a solution for an anisotropic medium with uniform diffusivity:

$$M(t) = M(0) \exp\left(-\int_0^t \mathbf{k}(u)^T\, \underline{D}\mathbf{k}(u)\, du\right) \quad [24]$$

Above, $M(0)$ is the amplitude of the initial transverse magnetization (at $t - 0^+$) just after the 90° pulse is applied.

For an isotropic medium the echo intensity, $M(\mathrm{TE})$, in a spin-echo experiment is then given by:

$$\frac{M(\mathrm{TE})}{M_0} = \exp\left(-D\int_0^{\mathrm{TE}} \mathbf{k}(t')\cdot\mathbf{k}(t')\,dt'\right). \quad [25]$$

This relation is valid for a spin-echo gradient pulse combination. If refocusing 180° rf pulses are used in the sequence, the sign of G is inverted for all gradient pulses following the 180° pulse. When only the diffusion sensitizing gradient pulses are present and $\delta \ll \Delta$, Eq. [25] simplifies to Eq. [12], as expected. Evaluating Eq. [25] becomes more complicated when many gradient pulses are involved, as in MR imaging. A useful quantity that characterizes the sensitivity of NMR sequences to diffusion is the "gradient factor," b, (13) defined as (14,15):

$$b = \int_0^{\mathrm{TE}} \mathbf{k}(t')\cdot\mathbf{k}(t')\,dt'. \quad [26]$$

The signal attenuation is then reduced to a simpler expression:

$$\frac{M(\mathrm{TE})}{M_0} = \exp(-bD). \quad [27]$$

One must remember that Eq. [25] is strictly valid for diffusion in infinite, homogeneous, and isotropic media. Then, no cross-terms exist between gradient pulses, i.e., the contributions to the measured NMR signal from each gradient axis are uncoupled, and may be determined separately (14). If diffusion is restricted by impermeable barriers, or if it is anisotropic, the signal attenuation must be calculated differently. As we will see, in anisotropic media, additional cross-terms must be taken into account in both diffusion spectroscopy and imaging (16).

NMR Diffusion Experiments: The Different Approaches

Several NMR diffusion sequences based on fundamental principles have been proposed in the literature, all of which are more or less compatible with NMR imaging. A more extensive analysis of the effects of diffusion in these sequences when used in the imaging mode will be given in the following chapters.

Constant Field Gradient Spin-echo Method

The effect of diffusion and other molecular translational motions on spin-echo signals in the presence of a constant background magnetic field inhomogeneity has already been described in Hahn's paper (17), and later analyzed by Carr and Purcell (18). If this inhomogeneity is a simple linear gradient G_0, or if such a gradient is purposely applied, the echo attenuation can easily be derived from Eq. [25] (Fig. 2) (18,19):

$$\frac{M(n\mathrm{TE})}{M_0} = \exp\left(\frac{-(\gamma G_0)^2 D\mathrm{TE}^3}{12n}\right), \quad [28]$$

where TE is the echo time, and n is the echo number in a multiple echo experiment. This technique gives the highest accuracy for the diffusion coefficient (20), provided that the relaxation time T_2 of the medium is not too short to allow enough diffusion attenuation to occur during TE. However, the diffusion time of this experiment is not well characterized. As spins diffuse for the duration of the sequence, i.e., TE, the effect of their displacement on the signal attenuation is a function of time, resulting in an "effective" diffusion time of only 2TE/3, as it can be seen by comparing Eqs. [28] and [12], where we assumed that $\delta = \Delta =$ TE/2 and $n = 1$.

Bipolar Gradient Pulse Spin-echo Technique

This technique, suggested by Stejskal and Tanner (10), is the most widely used sequence to measure diffusion by NMR. Equation [12] only gives an approximation of the echo attenuation, since the duration δ of each pulse may not be negligible as compared to the pulse interval Δ. The exact solution can be obtained from Eq. [25] (Fig. 2):

$$\frac{M}{M_0} = \exp(-(\gamma G\delta)^2\,(\Delta - \delta/3)\,D). \quad [29]$$

The residual background gradients G_0 that are constantly present during the sequence may also be taken into account, so that the signal attenuation is (10):

$$\begin{aligned}\frac{M}{M_0} = \exp(&-\gamma^2 D(t_1^2(t_2 - t_1/3)G_0^2 \\ &+\delta^2(\Delta-\delta/3)G^2 - \delta(t_1^2+t_2^2+\delta(t_1+t_2) \\ &+2\delta^2/3 - 2t_1t_2)GG_0))\end{aligned} \quad [30]$$

where t_1 is the time between the 90° pulse and the onset of the first gradient pulse, and t_2 is the time between the end of the second gradient pulse and the top of the echo. The terms containing G_0 may represent a significant contribution that can be difficult to evaluate. Equation [30] reduces to Eq. [12] if $\delta \ll \Delta$, and $G_0 \ll G$ (negligible background gradients). The diffusion time can be formally defined as $(\Delta - \delta/3)$ (10), but it is physically meaningful only when $\delta \ll \Delta$.

A classical source of error is to determine the diffu-

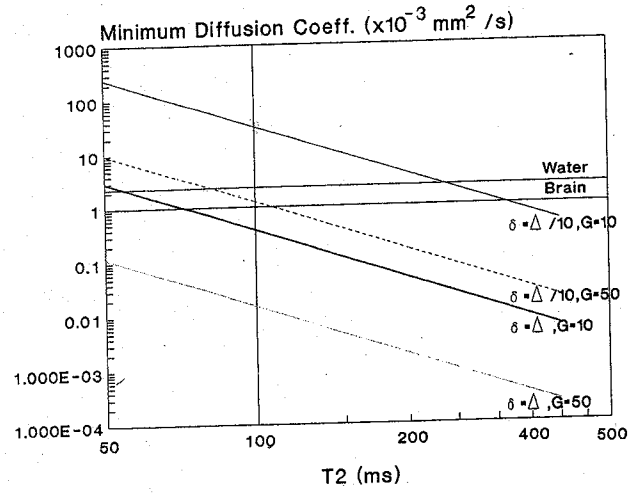

FIG. 4. Minimum measurable diffusion coefficient as a function of T_2 and gradient strength. The minimum diffusion coefficient measurable from a spin-echo sequence was calculated as a function of maximum gradient strength available (G = 10 mT/m or G = 50 mT/M) and T_2 in two different cases. The assumptions are that diffusion related echo attenuation must be at least 20% and that TE is equal to T_2, to maintain sufficiently high signal-to-noise ratio and good accuracy on diffusion. Best sensitivity is obtained for the constant gradient scheme ($\delta = \Delta$ = TE/2). It would be impossible to measure diffusion in brain (TE = 100 ms, $D = 1 \times 10^{-3}$mm^2/s) with short gradient pulses ($\delta = \Delta/10$), unless much larger gradients are used.

sion coefficient by this method when $\mathbf{k}(TE) \neq \mathbf{0}$. This produces an artifactual echo attenuation due to incomplete spin refocusing, which could be misinterpreted as arising from diffusion. In this sequence, any mismatch between the two gradient pulses (amplitude, G_1, G_2, and/or duration δ_1, δ_2) resulting in the condition that $G_1\delta_1 \neq G_2\delta_2$ will result in incomplete spin refocusing. Unfortunately, this mismatch naturally arises in the presence of background gradients or eddy currents. Tweaking gradients may ameliorate the problem. Nevertheless, careful hardware calibration is essential in diffusion NMR experiments.

To access the precision of this method, let us calculate the smallest diffusion coefficient one can measure using Eq. [29] given hardware limitations (maximum gradient strength achievable) and experimental constraints (diffusion time with respect to T_2). If we accept a 20% minimum signal attenuation and a 30% maximum signal loss from transverse relaxation to obtain reasonable accuracy for D, we find that the minimum measurable diffusion coefficient D_{min} is more than 16 times the diffusion coefficient of free water (Fig. 4):

$$D_{min} = 37 \times 10^{-3} \text{ mm}^2/\text{s} \qquad [31]a$$

with $\delta = \Delta/10$, $\Delta = T_2$, T_2 = 100 ms, and G = 10 mT/m. However, D_{min} is about $\frac{1}{5}$ the diffusion coefficient of water when different parameters are used:

$$D_{min} = 0.4 \times 10^{-3} \text{ mm}^2/\text{s} \qquad [31]b$$

with $\delta = \Delta$ (equivalent to a constant gradient), $\Delta = T_2/2$, T_2 = 100 ms, and G = 10 mT/m. Thus, T_2 is the main limiting factor of the accuracy of this method for a given available gradient power. The problem is further complicated by the fact that media with low diffusion coefficients generally have low T_2s owing to their low mobility. The accuracy of D, which can reach 1%, decreases with the signal-to-noise ratio. Tissues with short T_2s, as in the body, require short TEs that may not allow sufficient time to produce enough signal attenuation by diffusion. A solution to this problem is to use a scheme like the stimulated-echo sequence, which increases the effective diffusion time without signal attenuation by T_2 relaxation.

Stimulated Echo Technique

A stimulated echo is generated from a sequence consisting of three radiofrequency (rf) pulses separated by time intervals τ_1 and τ_2 (Fig. 5) (17). The remarkable feature of this sequence results from the magnetization evolution during the period τ_2 between the second and the third rf pulse. After the end of the second rf pulse, part of the transverse magnetization (exactly half in the case where 90° pulses are used) is stored as longitudinal magnetization, which becomes insensitive to field inhomogeneities and which decays according to T_1. As T_1 is usually much longer than T_2 in biological tissues, longer evolution times can be achieved than with a spin-echo sequence without the usual signal penalty due to T_2 decay. The third rf pulse returns the stored magnetization to the transverse plane at time τ_1 after the third pulse. The amplitude of the stimulated echo is, in the case where the three rf pulses are 90° pulses (17):

$$\frac{M}{M_0} = \frac{1}{2} \exp\left(-\frac{\tau_2}{T_1}\right) \exp\left(-\frac{2\tau_1}{T_2}\right). \qquad [32]$$

This property is particularly useful for diffusion measurements where long diffusion times are required. Gradient pulses must be inserted within the first and the third periods of the stimulated echo sequence (Fig. 5). The diffusion time then includes τ_2 and thus can be much longer than with a spin-echo sequence. The Stejskal-Tanner relation (Eq. [25]) still applies, provided that the period τ_2 is included in Δ (21). The longer diffusion time is useful in studying very slow diffusion rates or in compensating for unavailability of large gradients. Unfortunately, there is a signal reduction by one-half when compared to the spin-echo signal, since only half of the magnetization generated at the end of the τ_1 period contributes to the echo intensity. The stimulated echo scheme has been proposed for diffu-

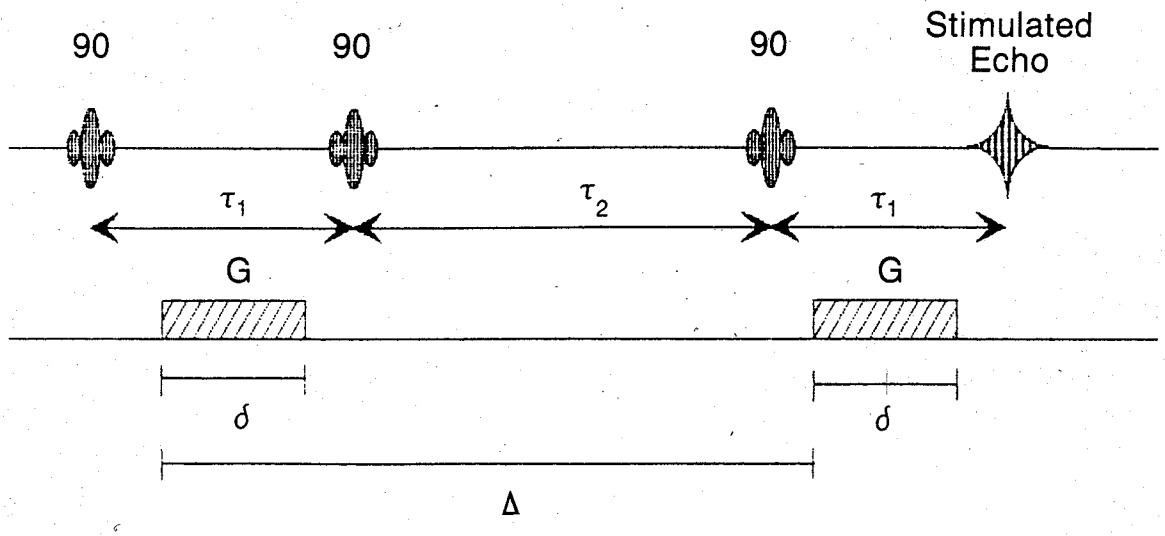

FIG. 5. Diffusion-stimulated echo sequence. A stimulated echo results from the spin excitation by three rf pulses separated by time intervals τ_1 and τ_2. During τ_2, relaxation is driven by T_1 and not by T_2. Since most often $T_1 \gg T_2$, τ_2 may be very long without signal-to-noise ratio penalty, by contrast with TE in a spin-echo sequence. Diffusion effects can be enhanced by placing gradient pulses within the τ_1 periods, where transverse magnetization is sensitive to field inhomogeneities.

sion imaging methods (22). Due to signal-to-noise considerations, it appears that this sequence is useful primarily in the presence of tissues with short T_2s or when the spin-echo sequence cannot be used (23).

Gradient Echo Technique

The effect of diffusion on the amplitude of a gradient echo formed by a bipolar gradient pulse pair of reversed polarity does not differ from that of a spin echo sequence. It is straightforward to use Eq. [25] in this case; it gives the same expression as Eq. [29]. However, a dramatic deviation from Eq. [29] can be seen if the gradient echo is part of a steady-state free precession (SSFP) sequence, where some degree of phase coherence is propagated throughout successive cycles, especially when low flip angles are used. Due to multiple echo paths that are then formed, a SSFP train can be considered for diffusion as a mixture of different schemes, i.e., gradient echo, spin echo, stimulated echo, and higher order echoes, with different diffusion times and different diffusion weightings. Kaiser et al. (24) have provided a detailed theoretical analysis of this problem. In the imaging domain, some work has been done, mainly using the CE-FAST scheme (25–28), with the hope that the speed of the SSFP techniques would decrease motion artifacts. Indeed, the effects of involuntary macroscopic motion are just as important as in spin-echo sequences, although ghosting is significantly reduced, because any motion related phase shift will propagate through all acquisition cycles. Moreover, the effects of diffusion and relaxation are no longer nicely separable in a multiplicative manner, as with spin echoes, so that diffusion measurements are always contaminated by relaxation effects (26,29).

Diffusion Measurements with B_1 Field Gradients

Diffusion gradients can also be developed by the rf (B_1) field produced by a NMR rf coil (30,31). It has been suggested that this method of producing diffusion gradients overcomes the hardware problems encountered when using strong static magnetic field (B_0) gradients. The idea is that an rf field gradient pulse $G_1 = dB_1/dr$ of duration δ, as induced by a surface coil oriented perpendicularly to the main transmit/receive NMR coil, will flip the magnetization within the sample by an angle Q which depends on position r:

$$Q = \gamma\delta \frac{dB_1}{dr} r. \qquad [33]$$

This flip angle dispersion, which should be made linear, is canceled after a time interval Δ using a symmetric rf pulse. As in the case of the B_0 gradient pulse sequence, moving spins will be incompletely refocused by the sequence, which results, here, in a loss of longitudinal magnetization. This longitudinal magnetization loss, M_z/M_0, can be probed using either an observed pulse (30) or an imaging sequence (31). This signal loss will depend on the diffusion coefficient and relaxation (T_1). With rf gradients, extremely short switching times can

be achieved, since there are no eddy currents. Furthermore, substantial gradient strength may be produced, depending on the output available from the rf transmitter, allowing measurements of very low diffusion coefficients. Unfortunately, such strong and long rf field pulses may result in high power deposition that may be incompatible with clinical use. Furthermore, the coil itself is subject to power dissipation problems that may alter its performance (tuning/matching, linearity) during the experiment.

DIFFUSION IN BIOLOGICAL SYSTEMS: EFFECTS OF MICRODYNAMICS AND MICROSTRUCTURE

Biological tissues differ largely from the condition of an "infinite, homogeneous medium" that we have considered so far. They are heterogeneous, containing multiple subcompartments (microstructure). Depending on the permeability of the barriers that divide these compartments, we have to consider exchange and transport between them (microdynamics). A classic treatment of the NMR signal may not properly reflect tissue structure or properties. Diffusion coefficients may be meaningless under these conditions if the measurement time scale or the measurement direction is not provided. The main difficulty is that the medium structure is generally not known in detail, so that modeling is required. In particular, one must be cautious to use Fick's law and derived relations (Eqs. [1]–[3]). The conditional probability distribution governing the diffusion process may now deviate from a Gaussian distribution appropriate for free diffusion (Eq. [11]). Most successful analyses start from the conditional probability distribution, taking into account the medium's structure and particular boundary conditions. We consider the simplest NMR sequence, the bipolar gradient spin echo sequence, in which the pulse duration δ is negligible with respect to pulse separation Δ. Equation [8], where now $P(z_1)$, the probability to find a spin initially at position z_1, has been incorporated, may be used as a starting point:

$$\frac{M}{M_0} = \int_{-\infty}^{\infty}\int_{-\infty}^{\infty} \exp(i\gamma G\delta(z_1 - z_2)) \times P(z_2 \mid z_1, \Delta)P(z_1)\, dz_1 dz_2 \qquad [34]$$

Another approach, suggested by Callaghan, and used by Cory et al. (32), is to invert this problem—to determine the probability distribution of the molecular displacements, $P(z, \Delta)$, from the NMR data. By rewriting Eq. [36] in a more suggestive form:

$$\frac{M(\gamma G\delta)}{M_0} = \int_{-\infty}^{\infty} \exp(i\gamma G\delta z)P(z, \Delta)\, dz \qquad [35]$$

we can see immediately that $P(z, \Delta)$ is the Fourier transform of the measured magnetization intensity. In measuring the displacement distribution, we make no *a priori* assumption that diffusion is free, and thus characterized by a Gaussian distribution with a single diffusion coefficient. Although apparent diffusion coefficients may be easier to use and understand, they may not always be meaningful, this is particularly true when there is complete restriction.

Restricted Diffusion

Diffusion is restricted when boundaries in the medium prevent molecules from moving freely across them (33–38). The observation of restriction must be related to the experimental parameters. When measurement times are very short, most molecules do not have enough time to reach boundaries, so that they behave as though they were diffusing freely. As the diffusion time increases, however, a larger fraction of molecules will strike the boundaries, and their displacement distribution will deviate from its behavior in an unbounded medium. The diffusion distance, $\sqrt{\langle z^2 \rangle}$ calculated for free diffusion using Einstein's relation $\sqrt{\langle z^2 \rangle} = \sqrt{2DT_d}$ (Eq. [5]) deviates from linearity with respect to $\sqrt{T_d}$, finally leveling-off as the diffusion distance reaches the size of the restricting compartment (Fig. 6). The effects of restriction will thus appear in the NMR signal when mean diffusion distances are

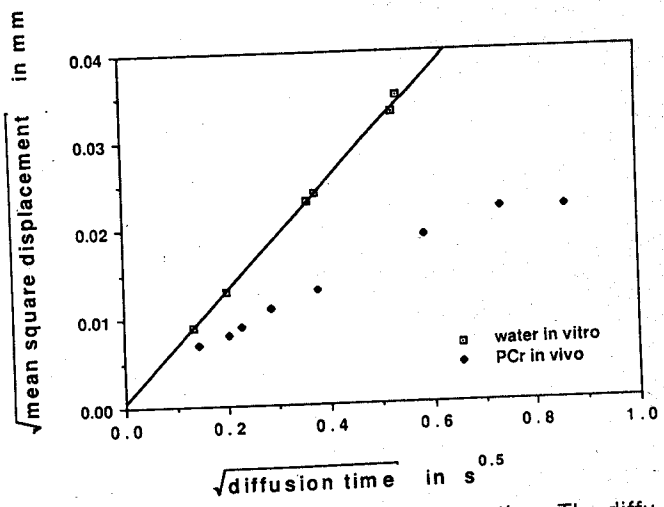

FIG. 6. Restricted diffusion and diffusion time. The diffusion distance is plotted against the square root of the diffusion time using Einstein's relation (Eq. [5]), similar to Fig. 1, for water *in vitro* and for phosphocreatine *in vivo* in rat muscle using ^{31}P spectroscopy. The leveling-off of the curve for phosphocreatine suggests that diffusion of this molecular species in muscle cell is restricted. The size of this restricted volume can be roughly estimated to 20 μm. (From Moonen et al., ref. 47, with permission.)

of the order of the characteristic length of the restricted compartment. These effects will depend on the type of restriction (impermeable or permeable barriers, attractive centers, etc.), the shape of the restricting volumes (spherical, cylindrical, planar, etc.), and the type of NMR experiment (constant or pulsed gradients), so that there is no single analytical expression to describe every configuration.

A simple example is represented by molecules diffusing between two impermeable parallel walls separated by a distance a (33). If the theoretical, free diffusion distance greatly exceeds a, the echo attenuation in the case of the bipolar gradient pulse experiment significantly deviates from an exponential decay and becomes independent of the diffusion time (33), implying that molecules are trapped in the direction of the applied gradient:

$$\frac{M(\gamma G\delta)}{M_0} = \left(\frac{\sin(\gamma G\delta a/2)}{(\gamma G\delta a/2)}\right)^2 \qquad [36]$$

For a constant gradient G_0, the attenuation is (34,36):

$$\frac{M(\gamma G\delta)}{M_0} = \exp(-(\mathrm{TE} - 17a^2/56\,D)a^4(\gamma G_0)^2/120\,D) \qquad [37]$$

Another interesting but more complicated case is represented by restricted diffusion in a spherical cavity of radius R_0. In the limit where the theoretical, free diffusion distance largely exceeds R_0, the attenuation is again independent of the diffusion time (33,36), so that the measured apparent diffusion coefficient decreases as the diffusion time is increased:

$$\frac{M(\gamma G\delta)}{M_0} = \exp\left(-\frac{(R_0\gamma G\delta)^2}{5\Delta}\right) \qquad [38]$$

corresponding to an asymptotic apparent diffusion coefficient $D_{\mathrm{asymp}} = R_0^2/(\Delta 5)$ with the factor 5 replaced by 3 when diffusion is confined to the surface of the sphere. For a constant gradient G_0, one obtains:

$$M/M_0 = \exp(-(\mathrm{TE} - 581R_0^2/1{,}260\,D)8R_0^4(\gamma G_0)^2/175\,D) \qquad [39]$$

Whatever the geometry of the restrictive medium, the deviation from linearity in the semilog plot of the signal attenuation versus b is crucial to determine whether diffusion is restricted, although other causes, such as diffusion in inhomogeneous systems, may produce the same effect. The ultimate test is to show that the measured diffusion coefficient D, or the signal attenuation varies with the diffusion time, T_d as it is changed. Such studies can, in principle, lead to the determination of the compartmental geometry and size of the restricting boundaries, but experiments are generally less ambitious. If one wants to avoid restricted diffusion effects, one must decrease the diffusion time $T_d(\Delta)$, so that the diffusion distance $\sqrt{\langle z^2\rangle}$ during $T_d(\Delta)$ remains less than the characteristic length, R of the restricted region. Unfortunately, the diffusion effect under these conditions becomes small, as can be seen from Eq. [29]. In order to produce more diffusion attenuation, one can use several pairs of gradient pulses. With this configuration (Fig. 7), the diffusion time remains Δ, the interval between two pulses of the same pair, but the b factor is n times larger than with a single pair, where n is the number of pulse pairs:

$$\frac{M}{M_0} = \exp(-(\gamma G\delta)^2(\Delta - \delta/3)\,Dn) \qquad [40]$$

while the b factor is, however, $\sqrt{n}$ times smaller than with a single pair.

Permeable Barriers

When the restrictive barriers become permeable to diffusing molecules, the qualitative features of the observed displacement distribution change. The mathematical treatment of diffusion in systems partitioned by permeable barriers is far from simple. An example was given by Tanner (39) in the case of equally spaced, plane barriers having a permeability constant κ. For short diffusion times, the apparent diffusion coefficient is the free diffusion coefficient D_0. As the diffusion time is increased, the apparent diffusion coefficient decreases, as expected for restricted diffusion, but it saturates at D_{asymp}, which depends on permeability (Fig. 8):

$$D_{\mathrm{asymp}} = \frac{D_0}{(1 - D_0/\kappa a)} \qquad [41]$$

where a is the barrier spacing, which can be estimated from the equivalent free diffusion distance that would be covered for a diffusion time $\sqrt{T_d}$, such that $D(\sqrt{T_d}) = (D_0 + D_{\mathrm{asymp}})/2$. It then becomes possible to estimate the barrier permeability κ (40). This approach, however, is oversimplified, given that the geometrical arrangement of the medium is generally unknown. In particular, this formalism does not apply to the case in which the system consists of spherical cavities separated by permeable barriers.

Anisotropic Diffusion

Diffusion is a three-dimensional process. However, molecular mobility may not be the same in all directions. This anisotropy may be due to the physical arrangement of the medium (liquid crystal) or to the presence of obstacles that limit diffusion (restricted

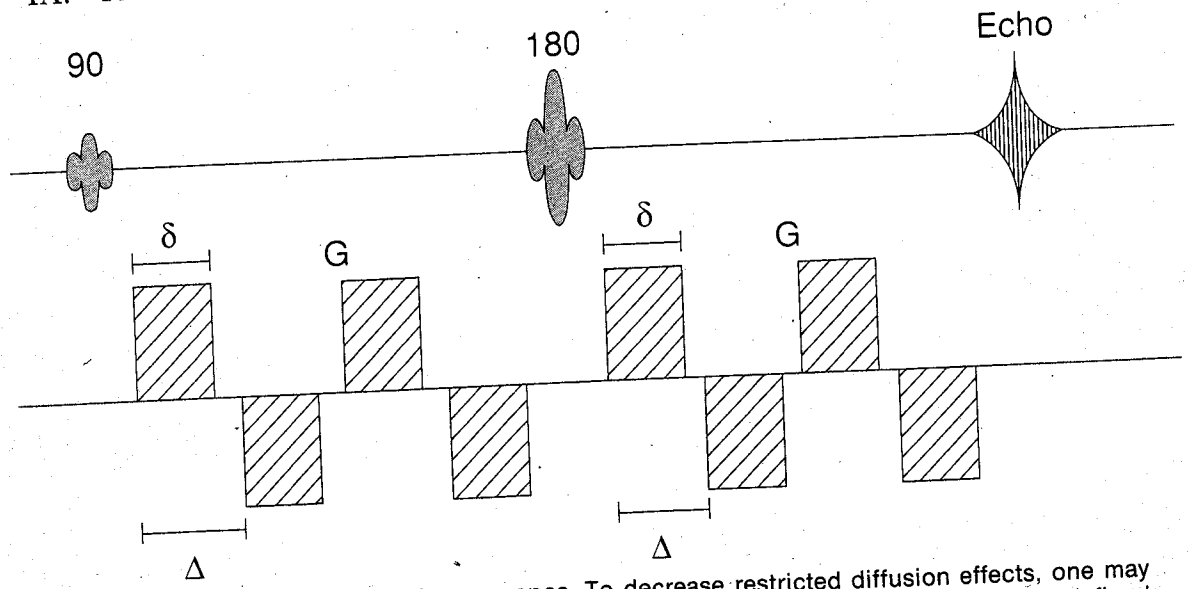

FIG. 7. Alternated gradient pulse sequence. To decrease restricted diffusion effects, one may use an alternating gradient pulse train. The diffusion time is, in this case, reduced to that defined by a single gradient pulse pair, i.e., $(\Delta - \delta/3)$. The b factor, however, is $\sqrt{n}$ times less than when using an equivalent single pair.

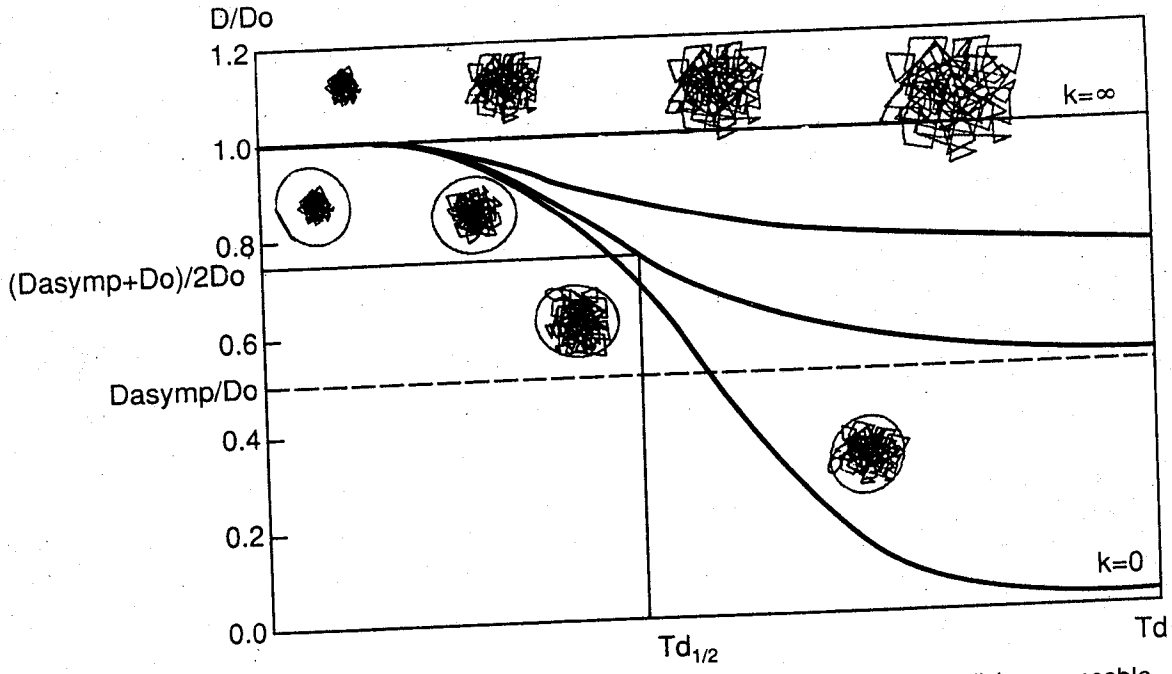

FIG. 8. Restriction by permeable barriers. When diffusion is reduced (restricted) by permeable barriers, the dependence of the diffusion coefficient on the diffusion time is modulated by the permeability of the restrictive barriers. In particular, the measured diffusion coefficient decreases with diffusion time, T_d, but saturates at a level, D_{asymp}. The size of the restrictive volume can be estimated from the freely diffusion distance that would be covered by free diffusing molecules during $\sqrt{T_d}$, where $\sqrt{T_d}$ is defined by the diffusion time corresponding to $D_{measured} = (D_{asymp} + D_0)/2$.

diffusion). It should be pointed out that diffusion can be both anisotropic and unrestricted. This behavior is well known in nematic liquid crystals (41) and can be found in the water lamellar phase of amphiphilic lyotropic systems (42) in which anisotropic diffusion measurements then could allow the determination of the transbilayer permeation rate. Moreover, structures that exhibit anisotropic diffusion at the molecular level can be isotropic at the microscopic level, resulting in a "powder average" effect that is difficult to sort out. The plot of log(M) versus b may not be linear in this case (42). This deviation from linearity can be ascribed, however, to anisotropy and not to restricted diffusion, because the diffusion measurements are independent of the diffusion time.

In anisotropic diffusion, the effective diffusion coefficient is replaced by an effective diffusion tensor (1). In this situation, Eq. [25] is no longer valid and the diffusion equations must be rewritten using a tensor formulation. In this case the term $\mathbf{k}(t)\cdot\mathbf{k}(t)\ D$ is replaced by the quadratic form, $\mathbf{k}(t)\cdot\underline{D}\cdot\mathbf{k}(t)$ (10). Equation [24] is used in place of Eq. [25], and Eqs. [26] and [27] must also be changed accordingly. The echo attenuation then becomes (16):

$$\frac{M(\mathrm{TE})}{M_0} = \exp\left(-\sum_{i=1}^{3}\sum_{j=1}^{3} b_{ij}\, D_{ij}\right) \qquad [42]$$

where b_{ij} is a b-matrix, and D_{ij} is an effective diffusion tensor (16). Its diagonal terms, D_{xx}, D_{yy}, and D_{zz}, reflect correlations between molecular displacements in the same directions, whereas its off-diagonal terms, D_{xy}, D_{xz}, D_{yz}, reflect correlations between molecular displacements in orthogonal directions. For instance, when observing diffusion in a lattice of semi-permeable parallel layers that are oriented obliquely with respect to the x and y axes, *macroscopic* displacements along x will appear to be correlated to displacements along y.

In general, we must assume that both diagonal and off-diagonal terms in the diffusion tensor do not vanish, unless we know *a priori* that the gradient (laboratory coordinate) directions coincide with the principal directions of the material—a condition which is rarely satisfied, especially in NMR imaging applications. Referring to Eq. [42], if diffusion gradients are applied simultaneously along the x, y, and z axes, the measured attenuation will now be a mixture of terms containing both diagonal and off-diagonal elements of the diffusion tensor. The specific problems associated with measurement and assessment of anisotropic diffusion data will be analyzed in greater detail in Chapter 8.

Diffusion in Multiple Compartment Systems

Most diffusion measurements in biological tissues are of an "apparent" diffusion coefficient. It is generally assumed that there is a unique diffusion coefficient in each measurement volume (voxel in imaging). We should now check to see if this assumption is valid, since most tissues consist of multiple subcompartments, including at least intracellular and extracellular compartments. Assuming that measurement times are short, so that diffusion is unrestricted in each subcompartment i, and that there is no exchange, the signal attenuation is:

$$\frac{M(\mathrm{TE})}{M_0} = \sum_{i=1}^{N} p_i \exp(-b\, D_i) \qquad [43]$$

where p_i is the density of molecules diffusing in compartment i, D_i is the associated diffusion coefficient, and N is the number of subcompartments. In this case, the "apparent" diffusion coefficient that would be measured would depend on the range used for the b values and would not reflect properly the diffusion in the voxel. Measurements with low b values would then be more sensitive to fast diffusion components. The ideal approach would be to separate all subcompartments by fitting the data with a multiexponential decay. Unfortunately, the values for D_i are often low and not very different from each other, so that large b values and high signal-to-noise ratios would be required. Furthermore, one would have to consider relaxation effects if compartments have different relaxation rates (43).

A different situation occurs when measurement times are longer. First, restricted diffusion may appear in the smallest subcompartments. Second, molecular exchanges may be seen between communicating compartments, so that the analytical treatment becomes difficult. Applying the central limit theorem for N compartments in the case of long diffusion times, one can justify the use of a single apparent diffusion constant D_a:

$$D_a = \sum_{i=1}^{N} p_i\, D_i \qquad [44]$$

This approach is also consistent with NMR dispersion studies (44) that suggest that cell membranes can be ignored on the NMR time scale. In intermediate situations, one must take into account the geometrical arrangement and the diffusion coefficients of each compartment, as well as their rates of exchange (45). A comprehensive analysis of the diffusion attenuation curves obtained with different diffusion times may lead to an accurate description of the medium microstructure.

Diffusion of Metabolites

Recent progress made in *in vivo* Fourier NMR spectroscopy allows the extension of diffusion measure-

ments to molecules other than water. NMR can resolve different nuclear species, because they have different Larmor frequencies. For different nuclear species, such as ^{31}P, ^{19}F, ^{2}H, or ^{13}C, one can make use of their chemical shift to determine independent diffusion coefficients of compounds in complex mixtures (46). Diffusion of phosphocreatine, for instance, can be studied by ^{31}P spectroscopy (47,48). Phosphocreatine is a true intracellular space probe (in contrast to water which diffuses across cell membranes), that exhibits true restricted diffusion (Fig. 6). Phosphocreatine (or *N*-acetylaspartate in neurons) may be used to provide information about the intracellular milieu, such as intercellular viscosity or geometry. Monitoring exchange of metabolites or drugs through cell membranes could also benefit from similar techniques designed to measure molecular flow (49). It is worth mentioning that, for nuclear species with spin $> \frac{1}{2}$ or for coupled spin systems, multiple quantum experiments would be less demanding on gradient hardware for diffusion measurements, because the effective gradient amplitudes that apply are increased by the power of the coherence order n. With $n = 2$, one thus expects a fourfold increase in the diffusion effect. Examples of such studies have been obtained with ^{23}Na (50) and in coupled spin systems (51) and have been used recently *in vivo* for lactic acid (52). The feasibility of measurements of metabolite diffusion *in vivo* using ^{1}H-NMR spectroscopy has recently been shown in animals (53) and in the human brain (54), as will be shown in Chapter 3.

REFERENCES

1. Crank J. *The mathematics of diffusion*. Oxford, England: Oxford University Press; 1975.
2. Jost W. *Diffusion in solids, liquids, gases*. New York: Academic Press; 1960.
3. Hervet H, Urbach W, Rondelez E. Mass diffusion measurement in liquid crystals by a novel optical method. *Journal of Chemical Physics* 1978;68:2725–2729.
4. Paulson OB, Hertz MM, Bolwig TG, Lassen NA. Filtration and diffusion of water across the blood-brain-barrier in man. *Microvasc Res* 1977;13:113–124.
5. Nicholson C, Phillips JM. Ion diffusion modified by tortuosity and volume fraction in the extracellular microenvironment of the rat cerebellum. *J Physiol* 1981;321:225–257.
6. Einstein A. *Investigations on the theory of the Brownian movement*. New York: Dover; 1926.
7. Abragam A. *Principles of nuclear magnetism*. London: Oxford University Press; 1961.
8. Bloembergen N, Purcell EM, Pound RV. Relaxation effects in nuclear magnetic resonance absorption. *Physical Review* 1948; 73:679.
9. Gandjbakhche AH, Nossal R, Bonner RF. Resolution limits for optical transillumination of abnormalities deeply imbedded in tissues. *Med Physics* 1994;21:185–191.
10. Stejskal EO, Tanner JE. Spin diffusion measurements: spin echoes in the presence of time-dependent field gradient. *Journal of Chemical Physics* 1965;42:288–292.
11. Torrey HC. Bloch equations with diffusion terms. *Physical Review* 1956;104:563–565.
12. Bloch F. Nuclear induction. *Physical Review* 1946;70:460–474.
13. Le Bihan D, Breton E, Lallemand D, Grenier P, Cabanis E, Laval-Jeantet M. MR imaging of intravoxel incoherent motions: application to diffusion and perfusion in neurologic disorders. *Radiology* 1986;161:401–407.
14. Le Bihan D. Magnetic resonance imaging of perfusion. *Magn Reson Med* 1990;14:283–292.
15. Ahn CB, Cho ZH. A generalized formulation of diffusion effects in um resolution nuclear magnetic resonance imaging. *Med Phys* 1989;16:22–28.
16. Basser PJ, Le Bihan D, Mattiello J. Estimation of the effective self-diffusion tensor from the NMR spin echo. *J Magn Reson* 1994;(B)403:247–254.
17. Hahn EL. Spin-echoes. *Physical Review* 1950;80:580–594.
18. Carr HY, Purcell EM. Effects of diffusion on free precession in nuclear magnetic resonance experiments. *Physical Review* 1954; 94:630–638.
19. Woessner DE. Effects of diffusion in nuclear magnetic resonance spin-echo experiments. *Journal of Chemical Physics* 1961;34:2057.
20. Harris KR, Mills R, Back PJ, Webster DS. An improved NMR spin-echo apparatus for the measurement of self-diffusion coefficient: The diffusion of water in aqueous electrolyte solutions. *J Magn Reson* 1978;29:473–482.
21. Tanner JE. Use of the stimulated echo in NMR diffusion studies. *Journal of Chemical Physics* 1970;52:2523–2526.
22. Merboldt KD, Hanicke W, Frahm J. Self-diffusion NMR imaging using stimulated echoes. *J Magn Reson* 1985;64:479–486.
23. MacFall JR, Le Bihan D. Comparison of stimulated echo, spin echo, and steady state free precession pulse sequences for MR imaging apparent diffusion coefficients. *Radiology* 1988;169(P): 344.
24. Kaiser R, Bartholdi E, Ernst RR. Diffusion and field-gradient effects in NMR Fourier spectroscopy. *Journal of Chemical Physics* 1974;60:2966.
25. Le Bihan D. Intravoxel incoherent motion imaging using steady-state free precession. *Magn Reson Med* 1988;7:346–351.
26. Le Bihan D, Turner R, MacFall JR. Effects of intravoxel incoherent motions (IVIM) in steady-state free precession (SSFP) imaging. Application to molecular diffusion imaging. *Magn Reson Med* 1989;10:324–337.
27. Merboldt KD, Hanicke W, Gyngell ML, Frahm J, Bruhn H. Rapid NMR imaging of molecular self-diffusion using a modified CE-FAST sequence. *J Magn Reson* 1989;82:115–121.
28. Merboldt KD, Bruhn H, Frahm J, Gyngell ML, Hanicke W, Deimling DM. MRI of "diffusion" in the human brain: new results using a modified CE-FAST sequence. *Magn Reson Med* 1989;9:423–429.
29. Wu EX, Buxton RB. Effect of diffusion on the steady-state magnetization with pulsed field gradients. *J Magn Reson* 1990;90: 243–253.
30. Canet D, Diter B, Belmajdoub A, Braondeau J, Boubel JC, Elbayed K. Self-diffusion measurements using a radiofrequency field gradient. *J Magn Reson* 1989;81:1–12.
31. Karczmar GS, Twieg DB, Lawry TJ, Matson GB, Weiner MW. Detection of motion using B1 gradients. *Magn Reson Med* 1988; 7:111–116.
32. Cory DG. Measurement of translational displacement probabilities by NMR: an indicator of compartmentation. *Magn Reson Med* 1990;14:435–444.
33. Stejskal EO. Use of spin echoes in a pulsed magnetic-field gradient to study restricted diffusion and flow. *Journal of Chemical Physics* 1965;43:3597–3603.
34. Wayne RC, Cotts RM. Nuclear-magnetic-resonance study of self-diffusion in a bounded medium. *Physical Review* 1966;151: 264–272.
35. Tanner JE, Stejskal EO. Restricted self-diffusion of protons in colloidal systems by the pulsed-gradient, spin-echo method. *Journal of Chemical Physics* 1968;49:1768–1777.
36. Neuman CH. Spin echo of spins diffusing in a bounded medium. *Journal of Chemical Physics* 1974;60:4508–4511.
37. Cooper RL, Chang DB, Young AC. Restricted diffusion in biophysical systems. *Biophys J* 1974;14:161–177.
38. Tanner JE. Self diffusion of water in frog muscle. *Biophys J* 1979;28:107–116.

39. Tanner JE. Transient diffusion in system partitioned by permeable barriers. Application to NMR measurements with a pulsed field gradient. *Journal of Chemical Physics* 1978;69:1748–1754.
40. Von Meerwall E, Ferguson RD. Interpreting pulsed-gradient spin-echo diffusion experiments with permeable membranes. *Journal of Chemical Physics* 1981;74:6956–6959.
41. Moseley ME. Anisotropic solvent translational diffusion in solutions of poly (g-benzyl-L-glutamate). *Journal of Chemical Physics* 1983;87:18–20.
42. Callaghan PT, Soderman O. Examination of the lamellar phase of aerosol OT/water using pulsed field gradient nuclear magnetic resonance. *Journal of Chemical Physics* 1983;87:1737.
43. Von Meerwall ED. Interpreting pulsed-gradient spin-echo diffusion experiments in polydisperse specimens. *J Magn Reson* 1982;50:409–416.
44. Koenig SH, Brown RD, Spiller M, Lundbom N. Relaxometry of brain: Why white matter appears bright in MRI. *Magn Reson Med* 1990;14:482–495.
45. Zientara GP, Freed JH. Spin-echoes for diffusion in bounded, heterogeneous media: a numerical study. *Journal of Chemical Physics* 1980;72:1285–1292.
46. James TL, McDonald GG. Measurement of the self-diffusion coefficient of each component in a complex system using pulsed-gradient fourier transform NMR. *J Magn Reson* 1973;11:58–61.
47. Moonen CTW, van Zijl PCM, Le Bihan D, DesPres D. In Vivo NMR diffusion spectroscopy. ^{31}P Application to phosphorus metabolites in muscle. *Magn Reson Med* 1990;13:467–477.
48. Yoshizaki K, Seo Y, Nishikawa H, Morimoto T. Application of pulsed-gradient ^{31} P NMR on frog muscle to measure the diffusion rates of phosphorus compounds in cells. *Biophys J* 1982; 38:209–211.
49. van Zijl PCM, Moonen CTW, Kaplan O, Faustino P, Cohen JS. Complete separation of intracellular and extracellular information in NMR spectra of perfused cell cultures. In: *Abstracts of the Proceedings of the Society of Magnetic Resonance in Medicine*. Berkeley: Society of Magnetic Resonance in Medicine; 1990:851.
50. Zax D, Pines A. Study of anisotropic diffusion of oriented molecules by multiple quantum spin echoes. *Journal of Chemical Physics* 1983;78:6333–6334.
51. Kay LE, Prestegard JH. An application of pulse-gradient double-quantum spin echoes to diffusion measurements on molecules with scalar-coupled spins. *J Magn Reson* 1986;67:103–113.
52. Sotak CH. A method for measuring the apparent self-diffusion coefficient of in vivo lactic acid using double quantum spectroscopy. *J Magn Reson* 1990;90:198–204.
53. Merboldt KD, Hostermann D, Hänicke W, Bruhn H, Frahm J. Molecular self-diffusion of intracellular metabolites in rat brain in vivo investigated by localized proton NMR diffusion spectroscopy. *Magn Reson Med* 1993;29:125–129.
54. Posse S, Cuenod CA, Le Bihan D. Human brain: proton diffusion MR spectroscopy. *Radiology* 1993;188:719–725.